COMPUTING AND ALGORITHM INSIGHT
Volume 3, Issue 1, June 2025 | pp. 19-42
https://doi.org/10.63208/21018-113

OPEN ACCESS
Check for updates

A HYBRID CPFD AND MACHINE LEARNING APPROACH FOR PREDICTIVE MODELING OF INDUSTRIAL FCC RISER REACTORS

Zhao Jingru[1] ✉, Bakhytzhan Sagintayev[1], and Fatoumata Diallo[2]

Faculty of Innovative Technologies, Almaty Technological University, Almaty, Kazakhstan[1]; School of Engineering and Technology, Central Queensland University, Rockhampton, Australia[2]

ABSTRACT

This study presents a novel hybrid model designed to predict six key process variables in an industrial-scale fluid catalytic cracking (FCC) riser reactor: vacuum gas oil (VGO) conversion, outlet temperature, and yields of gasoline, LCO, light gases, and coke. The methodology integrates computational particle-fluid dynamics (CPFD) with artificial intelligence, using Barracuda Virtual Reactor 22.0® to solve first principle model (FPM) equations. Based on 216 simulations incorporating CREC-UWO catalytic kinetics, a comprehensive dataset was generated to train a machine learning algorithm. A multiple output feedforward neural network (FNN) was utilized to correlate reactor feeding conditions with output parameters, achieving an average regression coefficient of 0.83 and an overall RMSE of 1.93. This research demonstrates that combining CPFD simulations with ML significantly enhances predictive accuracy and process optimization, offering substantial advancements for industrial FCC operations.

Keywords: *FCC Riser Reactor, CPFD Simulation, Feedforward Neural Network, Hybrid Modeling, VGO Catalytic Cracking.*

CORRESPONDING AUTHOR:
Zhao Jingru
Faculty of Innovative Technologies, Almaty Technological University, Almaty, Kazakhstan
contact: *z.jingru@atu.kz*

ARTICLE HISTORY
Received : January 15, 2025
Final Revised : May 29, 2025
Accepted : June 20, 2025
Published : June 30, 2025

© 2025 The Author(s) | Published by Integra Academic Press | This article is an open access article and distributed under the terms and conditions of the Creative Commons Attribution (CC BY-SA) license.

1. | INTRODUCTION

In recent decades, the petroleum refining sector has encountered a simultaneous set of pressures, characterized by escalating demand for refined products, a deterioration in the quality of raw crude oil, and more rigorous environmental and product specifications. To mitigate these issues, refineries have committed significant capital to research and development (R&D), focusing specifically on the advancement of simulation and modeling techniques [1]. Central to these efforts is the fluid catalytic cracking (FCC) process, which has emerged as a primary subject of investigation within contemporary refinery research. The significance of this process is underscored by the fact that nearly 45% of total refinery-produced fuel is derived from the FCC unit and its associated auxiliary systems [2]. As a result, the FCC has transitioned into one of the most economically lucrative operations and a cornerstone reactor unit in modern industrial processing. The strategic importance of the FCC reactor is illustrated in Figure 1, which highlights its role as the hub of the refinery network, transforming gas oil feedstocks into essential outputs such as gasoline, heating oil, and fuel gas.

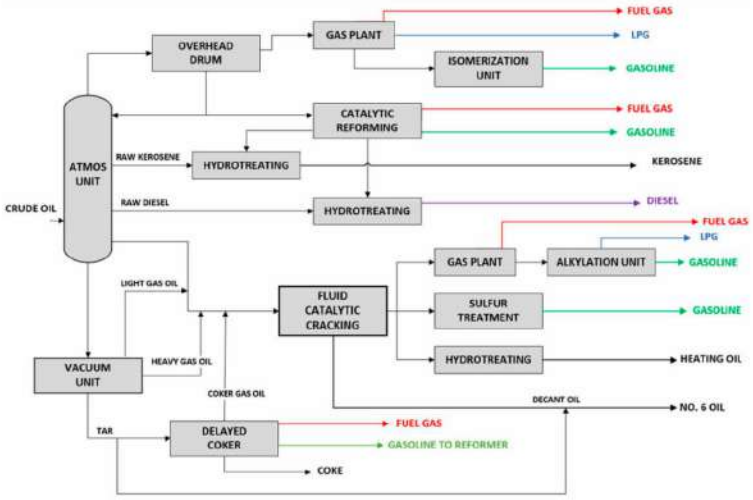


Figure 1. Illustration of the central function and strategic positioning of the FCC unit within contemporary petroleum refineries [2].

The FCC operation is comprised of three primary stages: (a) chemical reaction, (b) separation of products, and (c) regeneration of the catalyst. Throughout these phases, heavy gas oil feedstocks are transformed into lighter chemical fractions (C1–C4), alongside high-value components such as gasoline (C5+–C12) and cycle oils/diesel (C12–C16) [3,4]. The cracking reaction occurs within the riser reactor at near-atmospheric pressures and temperatures typically ranging from 500 to 570 °C. Within this unit, the heavy feedstock is introduced and cracked into lighter hydrocarbons through interaction with a specialized FCC catalyst [1]. Upon exiting the riser, these lighter fractions are conveyed to a fractionation system for separation and further processing. Concurrently, the catalyst experiences deactivation as coke deposits accumulate on its surface during the cracking process, thereby diminishing its catalytic efficiency. To mitigate this, a regeneration unit is utilized to combust the coke, restoring the catalyst's activity. Once regenerated, the catalyst is recirculated into the riser, maintaining the continuity of the FCC cycle [3].

Given the complexity of the underlying phenomena, substantial research has focused on improving the operational performance of FCC systems [5]. Nevertheless, modeling this process remains a formidable task due to the massive scale of the equipment, the intricate multiphase hydrodynamics, and the sophisticated kinetic mechanisms governing both cracking and regeneration [6]. Consequently, there is a critical need for process models capable of accurately simulating the myriad of variable interactions found in industrial-scale units. Significant progress has been made in developing first principle models (FPMs) for industrial FCC simulation [7]. These FPMs incorporate industrial dimensions and address various aspects such as steady-state conditions [8], dynamic responses [9,10], control strategies [11,12], and the complex hydrodynamics of transported-bed reactors through computational fluid dynamics (CFD) [13]. However, traditional FPMs face limitations, particularly regarding the intense coupling between reactor and regenerator variables [14] and the significant uncertainties associated with kinetic parameters [15]. As a result, achieving precise industrial models with reasonable computational costs using only FPMs remains a significant challenge.

To overcome the constraints of conventional methodologies, several alternatives have been explored over the last two decades. Initial efforts focused on integrating artificial intelligence (AI) into FCC modeling [14,16,17,18]. Furthermore, advancements in optimization and control techniques [3], paired with rapid computational progress, have spurred the development of various data-driven models (DDMs) and hybrid models (HMs) [5]. As illustrated in Figure 2, HMs—often termed "gray box" models—represent a synthesis of FPMs, which are grounded in rigorous phenomenological knowledge of fluid dynamics and kinetics, and DDMs, which rely heavily on empirical process data [19]. By merging these approaches, HMs aim to bridge the gaps in FPM and DDM methodologies, utilizing physicochemical constraints derived from chemical engineering principles alongside available data [20].

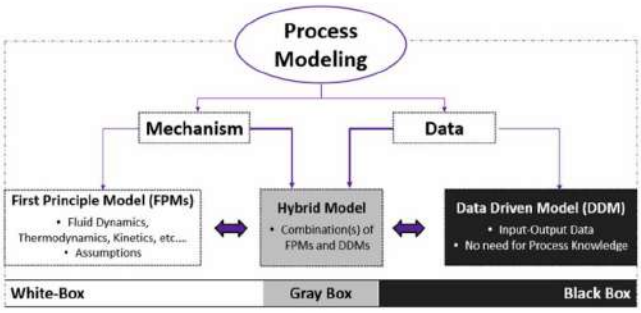


Figure 2. Classification of process modeling approaches [19].

HMs for FCC units have been predominantly designed by integrating machine learning (ML) algorithms with FPMs to yield models that are simultaneously simpler, more adaptable, precise, and interpretable for industrial applications [20,21,22]. The technical literature indicates that common applications for these ML algorithms involve the prediction, monitoring, control, and optimization of FCC processes [5]. However, it is important to observe that despite the variety of reported algorithms, selecting the most suitable one for a specific FCC unit or set of operating conditions remains difficult, especially when considering the diversity in feedstock properties, catalyst types, and catalyst-to-oil ratios.

Furthermore, driven by recent breakthroughs in numerical algorithms and the rapid expansion of computing power [23], CFD techniques are increasingly being adopted for FCC applications. This surge in interest is due to the ability of CFD to deliver comprehensive gas-solid hydrodynamic data for fluidized beds more efficiently and cost-effectively than conventional experimental methods [24]. Nonetheless, for the multiphase flows characteristic of FCC risers, standard CFD methods utilizing Eulerian-Eulerian frameworks often face limitations when applied to industrial-scale equipment. To address this, the Eulerian-Lagrangian multiphase flow model proposed by [25], known as computational particle-fluid dynamics (CPFD), was employed. This approach has gained considerable traction lately, owing to its proficiency in modeling large-scale units and its utility in optimizing multiphase gas-solid catalytic reactors [26].

In light of these considerations, the objective of the present research is to develop and execute hybrid AI models tailored for FCC systems. To achieve this, the following specific goals were established:

1. The formulation and execution of a robust CPFD model to simulate an industrial-scale FCC riser reactor, incorporating reliable kinetic data validated in a CREC riser simulator.
2. The creation of AI-driven models to forecast the performance of the FCC riser unit across an extensive spectrum of standard operational conditions. To the best of our knowledge, the existing literature does not yet contain a study that addresses this critical subject in such a comprehensive manner.

2. | METHODOLOGY

This paper presents a hybrid modeling framework developed to forecast six essential process variables within an industrial-scale FCC riser reactor: (a) vacuum gas oil (VGO) conversion, (b) riser outlet temperature, and the yields of (c) light cycle oil (LCO), (d) gasoline, (e) light gases, and (f) coke. The methodology synthesizes CPFD techniques with ML algorithms to determine the relationships between the initial feeding conditions of the riser and the subsequent output parameters of the catalytic reaction. As illustrated in Figure 3, this integrated approach enables the estimation of numerous operational scenarios with a substantial reduction in computational demand, decreasing processing times from several hours for standalone CPFD simulations to just a few minutes.

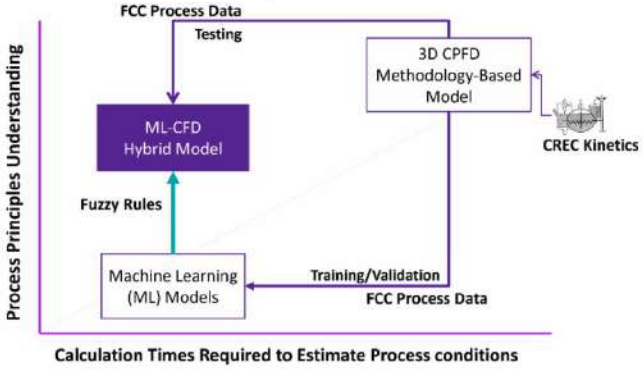


Figure 3. Proposed hybrid AI framework utilizing 3D CPFD simulations and CREC kinetics for the development and validation of industrial FCC predictive models.

As illustrated in Figure 3, the utilization of 3D CPFD simulations for a commercial-scale riser unit enables the creation of an extensive database. These 3D CPFD calculations incorporate VGO cracking kinetics established through experimental studies in a specialized minifluidized CREC riser simulator [27]. In parallel, the ML component integrates pertinent fuzzy rules derived from existing expertise to categorize specific variables within the hybrid AI model into low, medium, and high fuzzy values.

Based on this framework, the hybrid AI model in this research was developed and executed by allocating 90% of the generated dataset for training purposes, while the remaining 10% was reserved for model validation. Additionally, for each AI model configuration assessed, the coefficient of determination (R^2) was determined as a metric for establishing the reliability and predictive performance of the model.

2.1. Computational Particle-Fluid Dynamics (CPFD)

The CPFD approach employs a Lagrangian-Eulerian framework designed for the simulation of complex fluid-particle flows. This methodology utilizes a 3D multiphase particle-in-cell (MP-PIC) technique to resolve the governing equations for both fluids and particles across three dimensions. This process characterizes particle-fluid dynamics through the application of averaged Navier–Stokes equations, ensuring a robust coupling with the solid phase [25,28]. Within this framework, the transport of the solid phase is represented by a particle distribution function f. This function correlates the local particle number density with the spatiotemporal properties of the solids, including particle position x_p, velocity u_p, mass m_p, and time t [24,29], expressed as $f(x, u_p, m_p, t)$.

Fluid-Phase Equations

Continuity equation of fluid phase:

$$\frac{\partial(\varepsilon_f \rho_f)}{\partial t} + \nabla \cdot (\varepsilon_f \rho_f u_f) = \delta \dot{m}_p \tag{1}$$

Momentum equation of fluid phase:

$$\frac{\partial(\varepsilon_f \rho_f u_f)}{\partial t} + \nabla \cdot (\varepsilon_f \rho_f u_f u_f) = \begin{matrix} \text{Model A:} & -\nabla p_f + F + \varepsilon_f \rho_f g + \nabla \cdot (\varepsilon_f \tau_f) \\ \text{Model B:} & -\varepsilon_f \nabla p_f + F + \varepsilon_f \rho_f g + \nabla \cdot (\varepsilon_f \tau_f) \end{matrix} \tag{2}$$

Enthalpy:

$$\frac{\partial(\varepsilon_f \rho_f h_f)}{\partial t} + \nabla \cdot (\varepsilon_f \rho_f h_f u_f) = \varepsilon_f \left(\frac{\partial p}{\partial t} + u_f \cdot \nabla p_f\right) + \phi - \nabla \cdot (\varepsilon_f q) + \dot{Q} + S_h + \dot{q_D} \tag{3}$$

Species transport:

$$\frac{\partial(\varepsilon_f \rho_f Y_{f,i})}{\partial t} + \nabla \cdot (\varepsilon_f \rho_f Y_{f,i} u_f) = \nabla \cdot (\rho_f D \varepsilon_f \nabla Y_{f,i}) + \delta \dot{m_{\iota,chem}} \tag{4}$$

Solid-Phase Equations

Liouville equation (untuk fungsi distribusi partikel f):

$$\frac{\partial f}{\partial t} + \nabla \cdot (f u_p) + \nabla_{u_p} \cdot (f \dot{u_p}) = 0 \tag{5}$$

Particle acceleration:

$$\dot{u_p} = \frac{du_p}{dt} = D_s(u_f - u_p) - \frac{1}{\rho_p}\nabla p_f + g - \frac{1}{\varepsilon_p \rho_p}\nabla \tau_p + \frac{\overline{u_p} - u_p}{2\tau_D} \tag{6}$$

Particle mass:

$$\delta \dot{m}_p = -\iiint f \frac{dm_p}{dt}\, dm_p\, du_p\, dT_p \tag{7}$$

Particle volume fraction:

$$\varepsilon_p = \iiint f \frac{m_p}{\rho_p} \, dm_p \, du_p \, dT_p \tag{8}$$

Particle energy:

$$C_V \frac{dT_p}{dt} = \frac{1}{m_p} \frac{\lambda_f Nu_{f,p}}{2r_p} A_p \left(T_f - T_p\right) \tag{9}$$

Fluid-Solid Interphase & Interaction

Momentum transfer between phases:

$$F = \iiint f \left\{ m_p \left[D_p \left(u_f - u_p\right) - \frac{1}{\rho_p} \nabla p \right] + u_p \frac{dm_p}{dt} \right\} dm_p \, du_p \, dT_p \tag{10}$$

Particle-particle collision normal stress model:

$$\tau_p = \frac{P_p \varepsilon_p^{\beta}}{\max[(\varepsilon_{cp} - \varepsilon_p), \alpha(1 - \varepsilon_p)]} \tag{11}$$

The CPFD methodology employs a discrete particle technique where the fluid phase is considered a continuum, while the solid catalyst particles are represented through Lagrangian computational groups known as "computational parcels" or "clouds" [26]. These parcels represent clusters of physical particles that possess identical characteristics, such as size, density, velocity, and temperature. By utilizing this approach, the model significantly minimizes computational requirements while still capturing essential catalyst-particle interactions. Furthermore, because the CPFD method maintains predictive accuracy even when utilizing coarse meshes, it allows for computationally feasible long-duration simulations and the adoption of relatively large time-steps, a distinct advantage over traditional CFD techniques [30].

In this research, the CPFD framework was executed using the Barracuda Virtual Reactor 22.0® software, integrating the following components:

- Physical properties of both the fluid and catalyst particles.
- Fluid momentum balances governed by averaged Navier–Stokes equations coupled with the solid phase.
- Interphase interactions modeled via an Energy Minimization Multiscale (EMMS) drag correlation.
- Solid-phase interactions represented by a particle stress function τ_p.
- Comprehensive enthalpy balances accounting for both gas and particle phases.
- The specific particle size distribution of the FCC catalyst.
- Appropriate reaction kinetics for FCC VGO cracking.

2.1.1. FCC Riser Unit

The central goal of the FCC riser flow simulation was to determine the concentrations of key oil species and assess overall reactor performance. This evaluation focused on (a) VGO conversion levels and (b) the yields of various hydrocarbon products generated through primary VGO cracking or secondary reactions of gasoline and cycle oils. Given that the degree of hydrocarbon cracking is fundamentally governed by gas-solid residence times, available catalyst surface area, species partial pressures, and heat transfer from the catalyst [31], a precise representation of the FCC riser requires an integrated account of kinetics, thermodynamics, and fluid dynamics. Such integration is essential for the accurate calculation of flow properties, including gas-phase species and catalyst concentrations. For this study, CPFD simulations were applied to an industrial-scale FCC riser with a diameter of 0.96–1.25 m and a total height

of 43 m. These dimensions were based on the Petronor S.A. refinery's FCC unit in Bilbao, Spain, as documented by [32].

The 3D geometry of the FCC riser was discretized using a uniform grid, resulting in approximately 300,000 computational cells. This industrial-scale model includes a catalyst prelifting section, a feed injection zone equipped with 12 nozzles, and a main reaction zone with a length of 32.5 m. The CPFD simulations were designed to capture the complex mixing of gas and solid phases alongside the simultaneous cracking reactions. Further architectural details of the simulated industrial riser unit are illustrated in Figure 4.

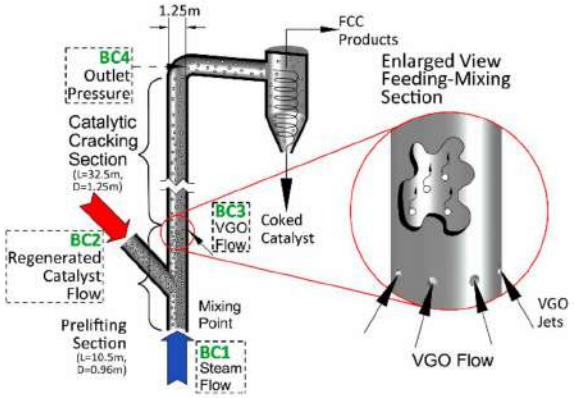


Figure 4. Geometry and boundary conditions (BC) of the FCC riser: BC1 (Steam), BC2 (Regenerated Catalyst), BC3 (VGO Feed), and BC4 (Outlet Pressure).

2.1.2. Operating Conditions

The Barracuda Virtual Reactor 22.0® software was utilized to develop a robust dataset of industrial-scale FCC simulations grounded in MP-PIC equations. This was accomplished by exploring an extensive spectrum of operational parameters, focusing on critical factors that influence the performance of the FCC riser, such as the catalyst-to-oil (C/O) ratio, various temperatures, and specific mass flow rates. To ensure the generation of high-quality, rigorous process data for the subsequent deployment of AI-based models, a total of 216 unique combinations of inlet conditions were evaluated. The specific variables and the representative ranges of conditions applied across these simulations are detailed in Table 1.

Table 1. Experimental Matrix for the Factorial Design of CPFD Simulations.

No.	Variables	Unit	Condition -1	Condition 0	Condition 1
1	Catalyst Mass Flow	kg/s	133.80	147.20	160.60
2	Catalyst Temperature	°C	-	650	700
3	VGO Mass Flow	kg/s	19.50	21.45	23.50
4	VGO Temperature	°C	210	230	250
5	Bottom Steam Mass Flow	kg/s	-	0.120	0.132
6	Bottom Steam Temperature	°C	-	250	300

In the setup for all CPFD simulations, the riser reactor was initially assumed to be filled with nitrogen, with the VGO mass flow starting at zero. Consequently, during the preliminary seconds of the simulation, only nitrogen is discharged from the unit while steam and catalyst particles move upward through the prelifting section. This steam-catalyst mixture subsequently contacts the feedstock, which is introduced via 12 injection nozzles. The VGO feed rate was

programmed to escalate gradually from 6 seconds, reaching its designated steady-state value at 13 seconds. For computational simplicity, the VGO was assumed to enter the riser in a vaporized state. Furthermore, a consistent initial coke concentration on the catalyst of 0.01 wt% was applied across all simulated conditions. These calculations modeled the reactor's start-up phase, extending until a total time-on-stream of 80 seconds was achieved.

Figure 4 delineates the specific boundary conditions (BCs) required for the CPFD framework, established at the riser's entry and exit points: (a) BC 1 defines the pressure, temperature, and mass flow for the incoming steam; (b) BC 2 specifies the corresponding parameters for the catalyst; (c) BC 3 sets the conditions for the VGO feed; and (d) BC 4 determines the pressure at the gas-solid outlet.

2.1.3. Catalytic Cracking Kinetics

Within the FCC riser, catalytic cracking transforms gas oil feedstocks (typically C21–C40) into a vast array of molecules ranging from C1 to C20. This shift in molecular weight increases the total number of moles, causing significant variations in volumetric flow as the mixture ascends the riser [33]. Consequently, incorporating precise cracking kinetics is vital for accurately modeling both the chemical transformations and the resulting hydrodynamics.

For this study, a 5-lump kinetic model for VGO cracking, which accounts for catalyst deactivation, was employed. This lumped approach categorizes the complex mixture into five pseudo-hydrocarbon components within the multiregime riser environment: (A) VGO (C26–C40), (B) LCO (C12–C16), (C) gasoline (C5+–C12), (D) light gases (C1–C4), and (E) coke, as illustrated in Figure 5.

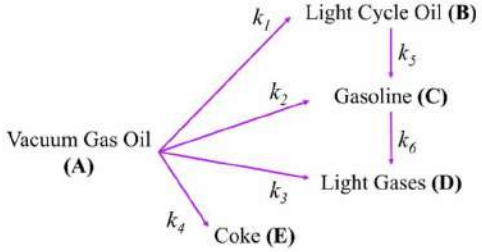


Figure 5. Reaction pathway for the five-lump kinetic model utilized in the FCC process.

Consequently, the VGO cracking kinetics are integrated into the CPFD framework through average cell size calculations. This process involves interpolating discrete properties from both fluid and particle phases onto the grid cells to determine the average values required for the chemical rate equations. Accordingly, reaction rates are determined within each cell by resolving a series of ordinary differential equations [28]. The reaction rate source/sink term for each specific lump i ($\delta m_{i,\dot{chem}}$), as referenced in Equation (4), is computed as follows [34]:

$$\delta m_{i,\dot{chem}} = \sum \delta_j r_j = \sum -\delta_j k_{0j} \exp\left(-\frac{Ea_j}{R_g T}\right) \rho_f \varepsilon_f m_p Y_{f,i}^n \quad (12)$$

In this expression, δ_j represents the stoichiometric coefficient for lump i within reaction path j, while r_j denotes the apparent reaction rate. The terms $Y_{f,i}$ and \$m_p\$ refer to the mass fraction of the lump and the catalyst mass per cell, respectively. R_g is the universal gas constant ($8.314\ \mathrm{J \cdot mol/K}$), T signifies the mean temperature of the phases, n is the reaction order, and k_0 and Ea are the pre-exponential factor and activation energy for each path j. For this research, kinetic parameters were adopted from [27], derived from VGO cracking experiments conducted in a CREC riser simulator.

2.2. AI-Based Model

The utilization of AI-based models for evaluating chemical process performance is gaining traction due to their inherent robustness, streamlined formulation, design simplicity, and adaptability [20]. As noted previously, AI methodologies can mitigate the limitations of FPMs when addressing highly nonlinear and complex systems. This has led to a significant surge in AI applications for modeling, optimization, control, and fault diagnosis in recent years [35]. Machine Learning (ML) algorithms, a branch of AI particularly suited for chemical engineering, have been explored for over three decades. Despite existing gaps in phenomenological understanding, these algorithms have delivered impressive results [19,36].

Generally, AI-based models developed via ML share core functions such as pattern recognition, logical reasoning, and decision-making. In chemical processing, these algorithms must frequently manage ill-defined problems, experimental noise, model uncertainty, and the requirement for rapid solutions to complex scenarios [36]. A critical phase in establishing an effective AI model involves identifying the correct input and output variables for the target system [35]. This allows the AI to characterize process behavior by accurately mapping the relationships between inputs and outputs [19].

In the present work, the AI model is built upon a set of input features comprising six independent inlet conditions and two dependent operating parameters, as detailed in Table 2. These eight predictors were selected to estimate six vital performance indicators of the industrial FCC riser: (a) VGO conversion, (b) LCO selectivity, (c) gasoline selectivity, (d) light gases selectivity, (e) coke yield, and (f) fluid outlet temperature.

Table 2. Proposed Input Features for the AI-Based Predictive Model.

No.	Condition	Units	Type
1	Catalyst Mass Flow	kg/s	Independent
2	Catalyst Temperature	K	
3	VGO Mass Flow	kg/s	
4	VGO Temperature	K	
5	Bottom Steam Mass Flow	kg/s	
6	Bottom Steam Temperature	K	
7	C/O Ratio	kg Catalyst/kg VGO	Dependent
8	Mixing Point Temperature	K	

To establish the AI-driven model, the dataset generated via CPFD simulations for the FCC riser unit was integrated into the MATLAB environment and processed according to the following protocol:

1. Initially, data points where mixing zone temperatures fell outside the 510–570 °C range were excluded. This step ensures consistency with the temperature constraints of the VGO cracking kinetics as documented by [27].
2. A "hold-out" strategy was then applied, wherein 90% of the filtered data was randomly assigned for AI training, while the remaining 10% was reserved exclusively for final model testing.
3. To address the limited size of the dataset, a 10-fold cross-validation technique was implemented, as recommended by [37]. In this phase, the training set was divided into 10 subsets, with 90% used for training and 10% for validation in each iteration.

4. The AI model was subsequently developed and validated across each of the defined K-folds.
5. Upon completion, the parameters from these individual folds were averaged to select the optimal configurations, resulting in an "ensemble" model characterized by consolidated statistical indicators.
6. The final performance of this "ensemble" model was verified against the 10% of original data previously set aside in step 2.

2.2.1. Artificial Neural Network (ANN)

Since the introduction of the backpropagation algorithm for training feedforward neural networks (FNNs) in 1986 and subsequent advancements in the early 1990s [36], ANNs have become one of the most prevalent ML algorithms in industrial applications. Their popularity stems from an exceptional capacity to discern complex, latent patterns within process input and output data [5]. Moreover, their ability to model highly nonlinear relationships through various activation functions has sparked significant interest across multiple chemical engineering domains [35]. In particular, FNN remains one of the most effectively utilized topologies in the technical literature and continues to be a preferred choice for sophisticated modeling tasks [21].

Fundamentally, ANNs are modeled after the structural and functional principles of the human brain. These networks consist of interconnected processing units, or nodes, organized into three distinct layers: the input layer, the hidden layer, and the output layer [20,38], as shown in Figure 6. The interactions between these nodes are weighted to represent the strength of the connections. Additionally, each neuron incorporates a bias term, which assists in adjusting individual node behavior and optimizing the overall predictive accuracy of the network.

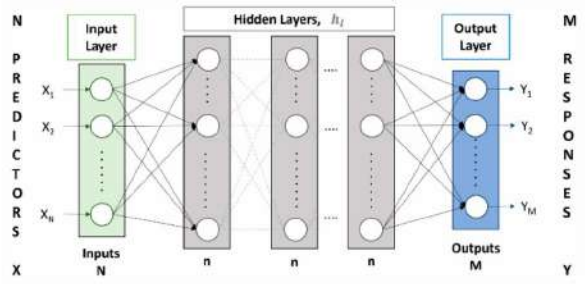


Figure 6. Structural layout of a multi-output feedforward neural network architecture.

As established by [39], the training phase of an FNN involves the continuous adjustment of weights and biases through iterative forward and backward computations. This procedure is maintained until a specified loss function reaches its minimum value [37]. Consequently, the identification of optimal hyperparameters is essential for effectively steering this iterative optimization. In this study, the efficacy of various FNN architectures was assessed using the averaged coefficient of determination (R^2) as the primary performance metric:

$$R^2(y,\hat{y}) = 1 - \frac{\sum_{i=1}^{n}(y_i-\hat{y}_i)^2}{(y_i-\bar{y})^2} \quad (13)$$

In this equation, y_i represents the output derived from the CPFD dataset, $\hat{y}_i$ denotes the predicted value from the model, and $\bar{y}$ is the mean of the observed values. The specific ANN hyperparameters utilized to construct the multiple output FNN are summarized in Table 3. These parameters, which encompass learning rates and activation functions, underwent

systematic tuning to ensure the minimization of the loss function during the training process. Notably, the total number of parameters within the FNN models was intentionally restricted to a maximum of 200. This constraint was implemented in light of the available data—comprising 216 operating scenarios and 6 output variables—to effectively balance model complexity and prevent the risks associated with parameter overfitting.

Table 3. Hyperparameter Settings and Optimization Configurations for FNN Development (MATLAB-designated Parameters).

Type	Hyperparameter	Value	Description
Performance	performFcn	RMSE	This provides the root mean square error (RMSE) as performance function.
	performParam.regularization	0.15	This considers a performance ratio for regularization.
	performParam.normalization	'standard'	This provides a standard normalization of the target variables values.
Training	trainParam.goal	0.01	This considers a RMSE desired value as the goal for the training.
	trainFcn	traingdx	This provides training by using gradient descent with momentum and adaptive learning rate backpropagation
	trainParam.lr	0.01	This considers an initial learning rate for the training.
	trainParam.lr_inc	1.005	This enhances training by employing an increase ratio in the learning rate.
	trainParam.lr_dec	0.05	This enhances training by employing a decrease ratio in the learning rate.
	trainParam.mc	0.75	This incorporates a momentum value for updating weights during training.
	divideFcn	'dividerand'	This involves training with a data division function for training and validation.
	divideParam.trainRatio	0.9	This considers a data split ratio for training.
	divideParam.valRatio	0.1	This considers a data split ratio for validation.
	trainParam.max_fail	20	This considers a maximum validation cap for failures.
Architecture	transferFcn	'tansig'	This involves a hyperbolic tangent sigmoid activation function for nodes connections.
	Hidden Layers	1, 2, 3	Up to a maximum of three hidden layers are considered.
	Hidden Layers Nodes	1–12	Up to a maximum of 12 nodes for each hidden layer are considered.
	Parameters	<200	Up to a maximum of 200 parameters are selected to prevent overparameterization.

2.2.2. Fuzzy Rules

In general, chemical processes can be rigorously represented through several methodologies, making it essential to differentiate between mechanistic descriptions, heuristic frameworks, and direct process data correlations [40]. Mechanistic approaches are founded upon rigorous mathematical equations derived from physical laws, whereas heuristic descriptions utilize empirical rules based on established prior expertise. In contrast, pure process data correlations are built strictly upon observed datasets. These varied strategies provide adaptability across different industrial scenarios, depending on the depth of phenomenological understanding and data availability.

Regarding the application of heuristic descriptions, fuzzy rule-based systems have emerged as robust instruments for characterizing the dynamic behavior of chemical processes [40]. Fuzzy logic, a multivalued logical framework, is exceptionally equipped to manage heuristically defined knowledge and qualitative rules [41]. Within this framework, fuzzy sets allow variables to be categorized into specific ranges, such as low, medium, and high values. The primary benefits of these descriptions include the ability to map and constrain process topology and define cause-effect relationships while bypassing the computational complexities often encountered when solving rigorous mathematical models via numerical simulation [16]. Furthermore, fuzzy sets are particularly advantageous for monitoring systems with highly volatile variables, as they provide boundaries that prevent potential miscalculation errors.

In this study, the following fuzzy sets were established to categorize the mixing temperature (T_{mix}) and the catalyst-to-oil (C/O) ratio:

1. Mixing Temperature Regimes:
    - Low Temperature Regime (LTR): $T_{mix} < 530$
    - Medium Temperature Regime (MTR): $530 < T_{mix} < 550$
    - High Temperature Regime (HTR): $T_{mix} > 550$
2. C/O Ratio Regimes:
    - Low CO Ratio: $C/O < 6$
    - Medium CO Ratio: $6 < C/O < 7.5$
    - High CO Ratio: $C/O > 7.5$

These fuzzy rules were implemented to classify the operating conditions into distinct regimes. Subsequently, these sets were utilized to augment the predictive accuracy of the FNN models, which were initially trained using continuous T_{mix} and C/O ratio values. The resulting performance improvements are detailed in the following sections.

3. | RESULTS AND DISCUSSION

3.1. CPFD Simulation Results

The CPFD simulations, executed within the Barracuda Virtual Reactor 22.0® environment, were utilized to analyze the complex gas-solid hydrodynamics and the associated temperature profiles within the industrial-scale FCC riser unit. To manage the computational demand, these simulations leveraged parallel computing and GPU acceleration through the Graham Cluster, a high-performance general-purpose computing resource provided by the Digital Research Alliance of Canada. The spatial distributions and contours resulting from the evaluation of the initial configuration of inlet conditions (Table 4) are illustrated in the following figures, specifically Figure 7, Figure 8, Figure 9, and Figure 10.

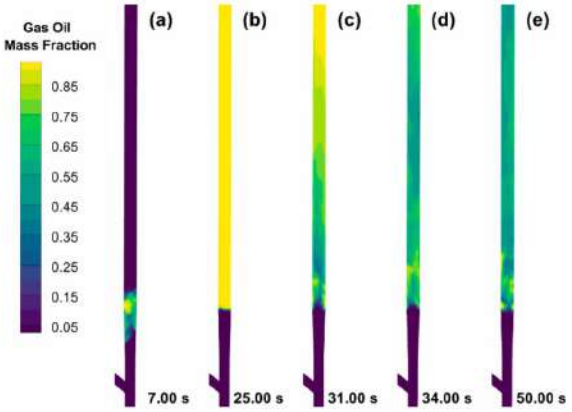


Figure 7. CPFD-simulated temporal evolution of VGO mass fractions at: (a) 7 s, (b) 25 s, (c) 31 s, (d) 34 s, and (e) 50 s.

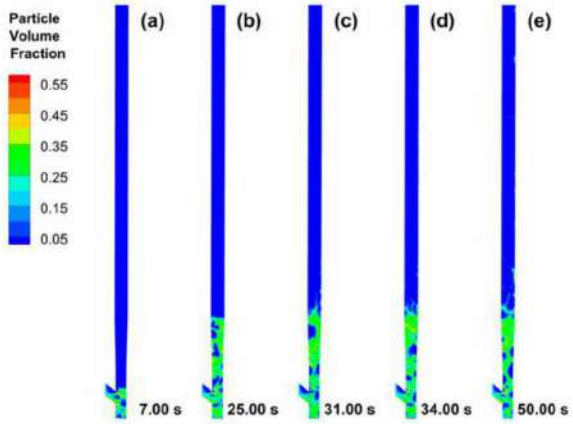


Figure 8. CPFD-simulated temporal evolution of catalyst volume fractions at: (a) 7 s, (b) 25 s, (c) 31 s, (d) 34 s, and (e) 50 s.

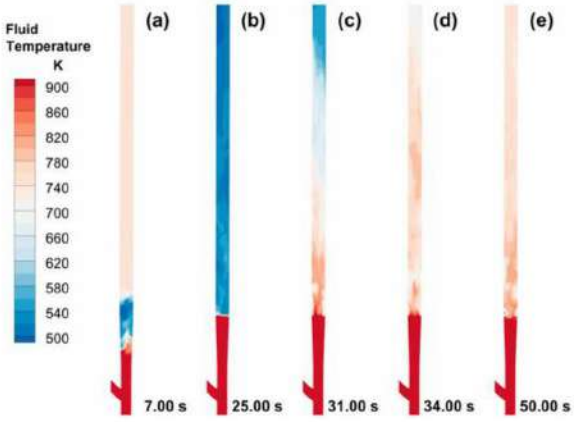


Figure 9. CPFD-simulated temporal evolution of fluid temperatures at: (a) 7 s, (b) 25 s, (c) 31 s, (d) 34 s, and (e) 50 s.

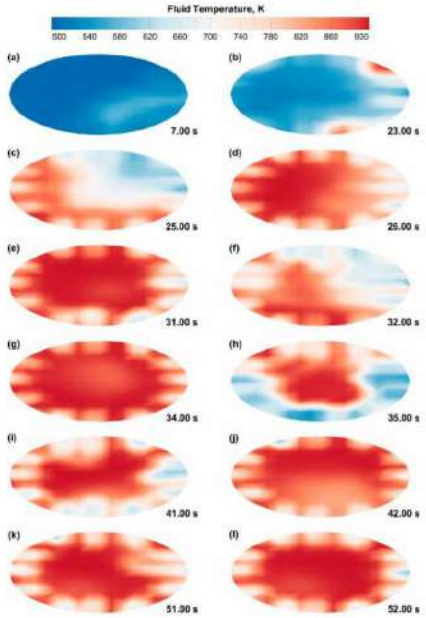


Figure 10. CPFD-simulated temporal evolution of mixing plane temperatures from 7 s to 52 s (a–l), displayed in descending order with shorter times on the left and longer times on the right.

Table 4. Primary Configuration of Inlet Parameters for Simulation ID: 1.

Condition	Value	Units
Catalyst mass flow	133.80	kg/s
Catalyst temperature	923	K
VGO mass flow	19.50	kg/s
VGO temperature	483	K
Bottom steam mass flow	0.120	kg/s
Bottom steam temperature	523	K

As depicted in Figure 7, the mass fraction of VGO remains at zero initially, followed by a significant increase at the 7-second mark of the simulation. This surge at the mixing level locations indicates the beginning of VGO feedstock introduction into the FCC unit. By 25 seconds of simulated reaction time, the entire reactor length is occupied by VGO. However, around 30 seconds, a decline in VGO mass fraction is observed, coinciding with the initial contact between catalyst particles and the injected VGO. This reduction signifies the onset of catalytic cracking reactions, leading to lower VGO concentrations as the flow ascends the riser. By 50 seconds, the VGO distribution at the outlet stabilizes, signaling the establishment of a quasi-steady state.

At the onset of the simulations, catalyst particles are fed continuously into the system. As shown in Figure 8 at 7 seconds, the catalyst occupies only a minimal portion of the prelifting zone with very low solid fraction levels. By 25 seconds, the particles are well-distributed, creating a densified phase throughout most of the prelifting section. After 30 seconds, the catalyst reaches the mixing point and interacts with the VGO, where the gas injections lift the particles. Consequently, two distinct regions emerge: a dense phase with high catalyst volume fractions in the lower section and a diluted phase with low volume fractions in the upper section, consistent with typical FCC riser hydrodynamics.

Figure 9 and Figure 10 illustrate the thermal dynamics during the CPFD-Barracuda simulations, highlighting the complex relationship between temperature profiles, VGO injection, catalyst distribution, and cracking kinetics. As observed in Figure 9, the prelifting zone maintains the highest thermal levels throughout the simulation due to the heat supplied by the regenerated catalyst (e.g., 923 K). As time progresses beyond 30 seconds, a descending temperature gradient along the riser height becomes evident. Higher temperatures are concentrated near the bottom mixing point, while lower temperatures are recorded at the outlet. This thermal reduction is primarily driven by the endothermic nature of the catalytic cracking reactions, which consume energy and induce a cooling effect.

Analysis of the mixing section's temperature (Figure 10) reveals several key trends. Initial temperatures are uniform, but fluctuations emerge at approximately 7 seconds as the VGO feed interacts with the steam-catalyst flow. At 23 seconds, the arrival of hot regenerated catalyst at the mixing zone moderates the endothermicity of the cracking process. By 25–26 seconds, the catalyst completely fills the mixing plane, with noticeably lower temperatures near the injection nozzles. Beyond 31 seconds, the hot catalyst continues to govern the thermal dynamics, albeit with temporal flow fluctuations. Eventually, a persistent thermal pattern emerges, indicating dynamic equilibrium. These findings emphasize the critical link between catalyst dynamics and temperature, highlighting the need to investigate catalyst recirculation and C/O ratios for optimal reactor performance.

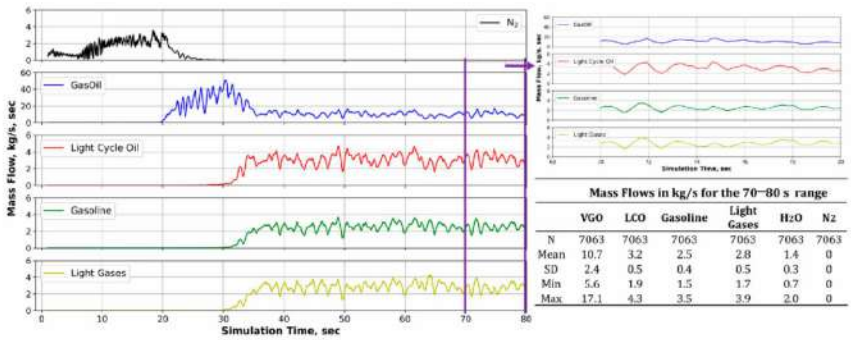
Furthermore, the data generated from the computations were rigorously analyzed using Python-based individual file processing. This allowed for the calculation of key performance variables at the riser outlet across various simulation intervals. Since mass fluxes for most chemical species stabilized after 60 seconds, the calculations for VGO conversion (X_{VGO}), product selectivity (S_i), and coke deposition (C_{Coke}) were performed based on the final 10 seconds of the simulation (70–80 s). The specific equations used are as follows:

$$X_{VGO} = \frac{F^0_{VGO} - F_{VGO}\backslash big|_{70-80\,s}}{F^0_{VGO}} \tag{14}$$

$$S_i = \frac{F_i\backslash big|_{70-80\,s}}{F^0_{VGO} - F_{VGO}\backslash big|_{70-80\,s}} \tag{15}$$

$$C_{Coke} = \frac{F_{Coke}\backslash big|_{70-80\,s}}{F_{Solids}\backslash big|_{70-80\,s}} \tag{16}$$

In these expressions, F^0_{VGO} and F_{VGO} represent the VGO inlet and outlet mass flows, respectively; F_i is the mass flow of product i; and F_{Solids} and F_{Coke} denote the total mass flows of solids and coke. The CPFD results and calculated variables for the first set of inlet conditions (Table 4) are presented in Figure 11 and Table 5.



Mass Flows in kg/s for the 70–80 s range

	VGO	LCO	Gasoline	Light Gases	H2O	N2
N	7063	7063	7063	7063	7063	7063
Mean	10.7	3.2	2.5	2.8	1.4	0
SD	2.4	0.5	0.4	0.5	0.3	0
Min	5.6	1.9	1.5	1.7	0.7	0
Max	17.1	4.3	3.5	3.9	2.0	0

Figure 11. Output data extraction from the CPFD simulation following 70 seconds of operational time.

Table 5. Key Performance Metrics and Thermal Outputs Derived from CPFD Simulations.

Variable of Interest	Value	Units
VGO conversion	45.19	%
LCO selectivity	36.34	%
Gasoline selectivity	28.87	%
Light gases selectivity	31.60	%
Mixing temperature	785	K
Outlet temperature	757	K

The data derived from the CPFD simulations were rigorously analyzed utilizing MATLAB R2022b. As detailed in Table 6, the CPFD-based predictions indicated a VGO conversion range spanning from moderate to high levels, specifically between 36.57% and 61.82%. Similarly, the recorded outlet temperatures fell within a moderate bracket of 785 to 831 K, which is consistent with the requirements for effective FCC riser reactor performance. Regarding product distribution, the selectivities documented in Table 6 suggest high riser efficiency, with the various target products being produced as intended. Furthermore, given that the CPFD simulations were initialized with a coke-on-catalyst value of 0.01%, the final calculated values, ranging from 0.5% to 0.66%, demonstrate the anticipated low to moderate coke accumulation on the catalyst surface resulting from the cracking reactions.

Table 6. Statistical Overview of Performance Indicators and Product Yields from CPFD Simulations.

Variable of Interest	Max	Min	Mean	SD	Units
VGO conversion	61.82	36.57	47.84	4.86	%
LCO selectivity	42.17	19.36	31.15	4.01	%
Gasoline selectivity	32.69	21.50	27.54	1.80	%
Light gases selectivity	40.81	23.57	33.15	3.48	%
Mixing temperature	869	754	814	24	K
Outlet temperature	831	742	785	20	K
Coke on catalyst	0.66	0.5	0.58	0.05	%

Figure 12 offers an extensive analysis of product selectivities and coke accumulation within the FCC riser unit, elucidating how these parameters correlate with VGO conversion levels. Initially, LCO selectivity demonstrates a distinct inverse relationship, where increasing VGO conversion rates consistently lead to a reduction in LCO selectivity. In contrast, gasoline selectivity maintains a relatively constant profile across the conversion spectrum, exhibiting only marginal fluctuations. Meanwhile, the selectivity for light gases follows a noteworthy upward trend at elevated VGO conversions, characterized by a more dispersed data distribution. Such variations in product yields suggest a propensity for overcracking within the riser under high-conversion scenarios, which ultimately shifts the product distribution toward lighter hydrocarbon fractions. Furthermore, the data for coke-on-catalyst indicates a clear segregation pattern, where higher coke levels are predominantly linked to increased catalyst inlet temperatures. This observed trend highlights the critical role of managing catalyst temperature to effectively control coke formation and optimize overall reactor efficiency.

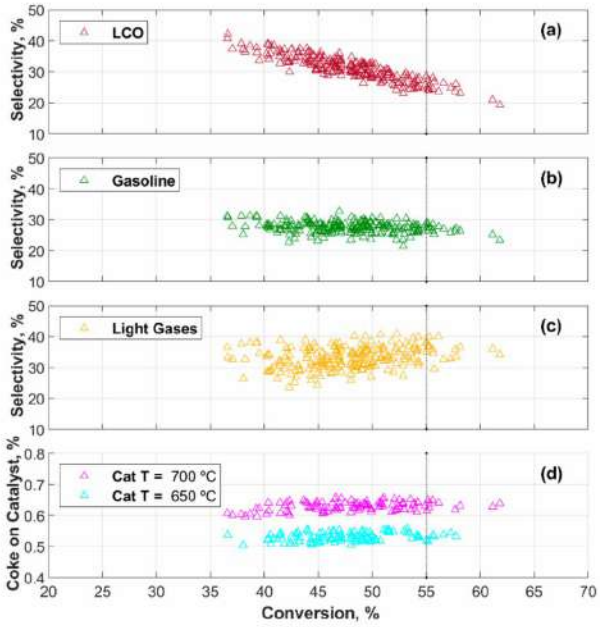


Figure 12. Selectivities vs. VGO conversion for 216 operating conditions simulated using CPFD-Barracuda Virtual Reactor® 22.0 software: (a) gasoline, (b) light gases, (c) LCO, and (d) coke-on-catalyst. Note: Cat T = catalyst temperature at riser inlet.

3.2. Machine Learning (ML) Results

In this research, a rigorous methodology was utilized to assess the performance of diverse FNN architectures, using the CPFD-generated dataset as the foundation for model testing. This was achieved by developing an averaged FNN ensemble based on the optimal parameters identified during the training of 10 k-folds for each specific architecture. This evaluative approach facilitated a robust comprehension of the AI model's performance while accounting for the variability inherent in different datasets. By analyzing the model's predictive capabilities across multiple folds, the risk of overfitting was effectively minimized, resulting in a more reliable representation of the model's ability to generalize to unseen data.

A significant finding from this evaluation is the substantial disparities observed in the overall root mean square error (ORMSE) across the various averaged FNN configurations. These discrepancies in ORMSE emphasize the high sensitivity of the models to both the underlying data distribution and the specific structural design of the neural networks. The fluctuations in ORMSE indicate that the selection of hidden layers and the number of neurons exert a profound influence on the model's predictive precision. Furthermore, variations were noted not only in the ORMSE metrics but also in the R^2 values for each individual product yield prediction. The performance results for the top five averaged FNN architectures are summarized in Table 7.

Table 7. Structural Configurations and Predictive Accuracy Metrics for the Five Highest-Performing Averaged FNN Architectures.

	FNN	FNN1	FNN2	FNN3	FNN4	FNN5
Architecture	Hidden Layers	1	2	2	3	3
	Nodes	[10]	[6, 9]	[10, 5]	[3, 10, 7]	[6, 10, 4]
	Parameters	156	177	181	192	198
ORMSE		2.38	2.00	1.98	2.37	2.24
R^2	VGO Conversion	0.86	0.86	0.85	0.80	0.85
	LCO selectivity	0.80	0.85	0.84	0.81	0.86
	Gasoline selectivity	0.09	0.15	0.17	0.23	0.29
	Light Gases selectivity	0.65	0.69	0.66	0.68	0.68
	Outlet Temperature	0.96	0.97	0.98	0.96	0.96
	Coke on Catalyst	0.96	0.99	0.99	0.99	0.99
Average R^2		0.721	0.752	0.749	0.745	0.772

On average, the evaluated models demonstrate consistent performance across most product yield predictions. These architectures differ primarily in their structural depth, specifically the number of hidden layers and neurons. Among the configurations tested, FNN3 and FNN2 exhibit the highest precision, yielding the lowest ORMSE values of 1.98 and 2.00, respectively. These results underscore the superior predictive accuracy of the 2-hidden-layer FNN framework. Notably, these specific networks maintain a relatively streamlined structure compared to the more intricate models, such as FNN4 (192 parameters) and FNN5 (198 parameters).

Furthermore, an examination of the R^2 values reveals distinct variations in how each architecture fits the simulated data. For example, the 1-hidden-layer FNN1 demonstrates excellence in modeling VGO conversion within the riser unit, achieving an R^2 of 0.86, yet it shows limited capability in predicting gasoline selectivity with an R^2 of only 0.09. The 2-hidden-layer models, FNN2 and FNN3, perform comparably to FNN1 regarding VGO conversion while providing marginal improvements in gasoline selectivity estimation. Similarly, although more complex architectures like FNN4 and FNN5 show further enhancements in gasoline selectivity prediction, the gains in average R^2 are relatively minor when contrasted with the 2-hidden-layer FNNs. These findings highlight the high sensitivity of FNN performance to architectural design and data distribution, reinforcing the necessity for meticulous selection and optimization in predictive modeling. The discrepancies in R^2 values across different target variables suggest that a universal architecture may not be sufficient for all modeling tasks.

Table 8 presents the modeling outcomes for four distinct FNN architectures that incorporate fuzzy set conditions for mixing temperature and C/O ratio. These fuzzy sets were integrated into the FNN models as dummy variables, introducing six additional variables into the input layer. These new parameters effectively replace the direct numerical values of T_{mix} and C/O ratio, consequently increasing the total parameter count due to the requirement for new nodes and their corresponding layer connections. For the FNN1 architecture, this structural adjustment increased the number of parameters from 156 (as shown in Table 7) to 196 (as shown in Table 8). Because this modification caused the FNN2, FNN3, FNN4, and FNN5 models to exceed the predefined limit of 200 parameters established in Section 2.2.1, 3-

hidden-layer architectures were excluded from further consideration. Instead, three new 2-hidden-layer FNN architectures were introduced for the subsequent model discrimination analysis.

Table 8. Structural Parameters and Predictive Performance of Averaged FNNs Incorporating Fuzzy Logic.

		FNN1	FNN2	FNN3	FNN4
Architecture	Hidden Layers	1	2	2	2
	Nodes	[10]	[5, 5]	[5, 8]	[8, 5]
	Parameters	196	131	167	185
ORMSE		1.78	1.93	2.02	1.93
R^2	VGO Conversion	0.84	0.85	0.85	0.89
	LCO selectivity	0.79	0.84	0.88	0.89
	Gasoline selectivity	0.37	0.14	0.68	0.49
	Light Gases selectivity	0.80	0.69	0.78	0.79
	Outlet Temperature	0.99	0.98	0.96	0.97
	Coke on Catalyst	0.99	0.99	0.99	0.99
Average R^2		0.796	0.749	0.859	0.836

As demonstrated in Table 8, the modifications to the proposed AI architecture lead to a noticeable enhancement in overall predictive performance. Specifically, the ORMSE values now fall within a more constrained range of 1.78 to 2.02, representing an improvement over the 1.98 to 2.38 range previously reported in Table 8. Similarly, the R^2 values of 0.859 and 0.836 achieved by the revised 2-hidden layer FNN3 and FNN4 models, respectively, indicate a significant increase compared to the values of 0.745 and 0.749 observed in Table 7. It is important to highlight that these gains in R^2 are primarily driven by the enhanced ability of the new FNN models to predict the distribution of gasoline and light gases selectivity. This predictive refinement is further evidenced by comparing the hydrocarbon lumps for the FNN1 model across Table 7 and Table 8, where the R^2 for gasoline and light gases selectivity rose from 0.09 and 0.65 to 0.37 and 0.80, respectively. Consequently, these results confirm the positive impact of integrating fuzzy rules and additional model variables into the FNN framework as part of the HM architecture proposed in this study.

Ultimately, the most appropriate FNN architecture was selected by balancing model complexity with predictive accuracy. The chosen configuration is the FNN4 model, which utilizes two hidden layers containing eight and five neurons, respectively. Figure 13 illustrates the high-fidelity predictions achieved for all considered output variables: (a) outlet riser temperature, (b) VGO conversion, (c) LCO selectivity, (d) gasoline selectivity, (e) light gases selectivity, and (f) coke-on-catalyst.

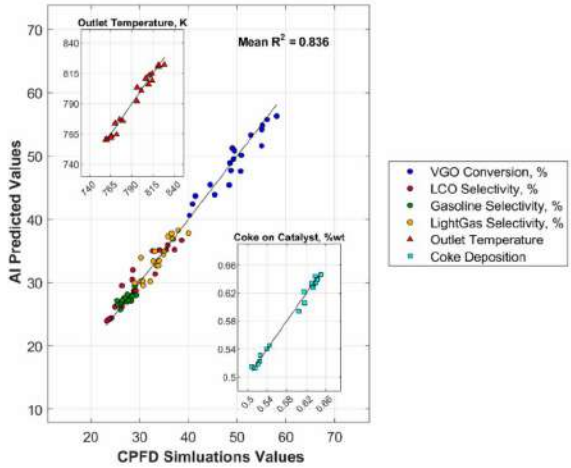


Figure 13. Parity plots comparing FNN predictions against CPFD simulation data for FCC riser reactor variables.

As illustrated in Figure 13, the FNN hybrid model, enhanced by fuzzy logic constraints, demonstrates strong alignment with the CPFD-Barracuda estimations. The minor deviations observed are attributed to inherent sources of computational and experimental error. Consequently, the proposed neural network model serves as a dependable and efficient analytical tool for predicting critical process variables in FCC riser reactor units. This predictive capability is achieved while offering a substantial reduction in computational overhead and processing time compared to full-scale simulations.

It is important to emphasize that the structural design of the FNN4 model is not inherently feedstock-dependent and possesses the flexibility to be adapted for different VGO feedstocks or FCC catalysts. Under such alternative conditions, the FNN4 would simply require retraining and validation using an appropriate new dataset. Building upon the successful outcomes of this research and the ongoing progress at CREC-UWO—specifically regarding new VGO cracking kinetics that account for C/O ratio influences in the new CREC Riser Simulator Mark II unit—it is expected that an updated hybrid AI model will be developed in the near future.

4. | CONCLUSIONS

The primary findings of this research are summarized as follows:

- CPFD simulations serve as an essential methodology for evaluating the performance of industrial-scale FCC riser reactors across a broad spectrum of potential operating conditions.
- The integration of CPFD simulations with CREC-UWO kinetics, derived from a minifluidized CREC riser simulator, significantly advances AI development by providing high-quality datasets for model training and rigorous validation.
- Incorporating fuzzy logic constraints into AI frameworks enhances the reliability and confidence of the proposed hybrid AI models for FCC applications.
- For FCC units, FNN architectures should be designed with a restricted number of hidden layers to ensure the total number of model parameters remains computationally tractable and manageable.
- Optimized FNN hybrid models for FCC units are capable of delivering superior performance estimations and accurate lump species predictions, characterized by high coefficients of determination (R^2).

REFERENCES

1. Pinheiro, C.I.C.; Fernandes, J.L.; Domingues, L.; Chambel, A.J.S.; Graça, I.; Oliveira, N.M.C.; Cerqueira, H.S.; Ribeiro, F.R. Fluid Catalytic Cracking (FCC) Process Modeling, Simulation, and Control. *Ind. Eng. Chem. Res.* 2012, 51, 1–29.
2. Sadeghbeigi, R. Fluid catalytic cracking process description—Converter section. In *Fluid Catalytic Cracking Handbook*; Elsevier: Amsterdam, The Netherlands, 2020; pp. 1–22.
3. Guan, H.; Ye, L.; Shen, F.; Song, Z. Economic operation of a fluid catalytic cracking process using self-optimizing control and reconfiguration. *J. Taiwan Inst. Chem. Eng.* 2019, 96, 104–113.
4. Zhang, X.; Zou, Y.; Li, S. Enhancing incremental deep learning for FCCU end-point quality prediction. *Inf. Sci.* 2020, 530, 95–107.
5. Khaldi, M.K.; Al-Dhaifallah, M.; Taha, O. Artificial intelligence perspectives: A systematic literature review on modeling, control, and optimization of fluid catalytic cracking. *Alex. Eng. J.* 2023, 80, 294–314.
6. Han, I.-S.; Chung, C.-B. Dynamic modeling and simulation of a fluidized catalytic cracking process. Part I: Process modeling. *Chem. Eng. Sci.* 2001, 56, 1951–1971.
7. Liu, A.Y.; Chang, A.-F.; Kiran, P. Predictive Modeling of the Fluid Catalytic Cracking (FCC) Process. In *Petroleum Refinery Process Modeling—Integrated Optimization Tools and Applications*; Wiley: Hoboken, NJ, USA, 2018; ISBN 9783527344239.
8. Olafadehan, O.A.; Sunmola, O.P.; Jaiyeola, A.; Efeovbokhan, V.; Abatan, O.G. Modelling and simulation of an industrial RFCCU-riser reactor for catalytic cracking of vacuum residue. *Appl. Petrochem. Res.* 2018, 8, 219–237.
9. Ali, H.; Rohani, S.; Corriou, J. Modelling and Control of a Riser Type Fluid Catalytic Cracking (FCC) Unit. *Chem. Eng. Res. Des.* 1997, 75, 401–412.
10. Kim, S.; Urm, J.; Kim, D.S.; Lee, K.; Lee, J.M. Modeling, simulation and structural analysis of a fluid catalytic cracking (FCC) process. *Korean J. Chem. Eng.* 2018, 35, 2327–2335.
11. Khandalekar, P.; Riggs, J. Nonlinear process model based control and optimization of a model IV FCC unit. *Comput. Chem. Eng.* 1995, 19, 1153–1168.
12. Arbel, A.; Huang, Z.; Rinard, I.H.; Shinnar, R.; Sapre, A.V. Dynamic and Control of Fluidized Catalytic Crackers. 1. Modeling of the Current Generation of FCC's. *Ind. Eng. Chem. Res.* 1995, 34, 1228–1243.
13. Araujo-Monroy, C.; López-Isunza, F. Modeling and Simulation of an Industrial Fluid Catalytic Cracking Riser Reactor Using a Lump-Kinetic Model for a Distinct Feedstock. *Ind. Eng. Chem. Res.* 2006, 45, 120–128.
14. Bollas, G.; Papadokonstadakis, S.; Michalopoulos, J.; Arampatzis, G.; Lappas, A.; Vasalos, I.; Lygeros, A. Using hybrid neural networks in scaling up an FCC model from a pilot plant to an industrial unit. *Chem. Eng. Process.-Process Intensif.* 2003, 42, 697–713.
15. Alaradi, A.; Rohani, S. Identification and control of a riser-type FCC unit using neural networks. *Comput. Chem. Eng.* 2002, 26, 401–421.
16. Wang, X.; Chen, B.; Yang, S.; McGreavy, C. Neural nets, fuzzy sets and digraphs in safety and operability studies of refinery reaction processes. *Chem. Eng. Sci.* 1996, 51, 2169–2178.
17. Yang, S.; Chen, B.; Wang, X. Neural network based fault diagnosis using unmeasurable inputs. *Eng. Appl. Artif. Intell.* 2000, 13, 345–356.

18. Michalopoulos, J.; Papadokonstadakis, S.; Arampatzis, G.; Lygeros, A. Modelling of an Industrial Fluid Catalytic Cracking Unit Using Neural Networks. *Chem. Eng. Res. Des.* 2001, 79, 137–142.
19. Zendehboudi, S.; Rezaei, N.; Lohi, A. Applications of hybrid models in chemical, petroleum, and energy systems: A systematic review. *Appl. Energy* 2018, 228, 2539–2566.
20. Ali, J.M.; Hussain, M.; Tade, M.O.; Zhang, J. Artificial Intelligence techniques applied as estimator in chemical process systems—A literature survey. *Expert Syst. Appl.* 2015, 42, 5915–5931.
21. Abdollahi, S.A.; Ranjbar, S.F.; Jahromi, D.R. Applying feature selection and machine learning techniques to estimate the biomass higher heating value. *Sci. Rep.* 2023, 13, 16093.
22. Zhang, M.; Yang, Z.; Zhao, Y.; Lv, M.; Lan, X.; Shi, X.; Gao, J.; Li, C.; Yuan, Z.; Lin, Y. A hybrid safety monitoring framework for industrial FCC disengager coking rate based on FPM, CFD, and ML. *Process Saf. Environ. Prot.* 2023, 175, 17–33.
23. Liang, Y.; Zhang, Y.; Lu, C. CPFD simulation on wear mechanisms in disk–donut FCC strippers. *Powder Technol.* 2015, 279, 269–281.
24. McIntyre, C.; Hughes, R.; Macchi, A.; Mehrani, P. Computational modeling of high pressure bubbling fluidized bed hydrodynamics using ilmenite particles. *Powder Technol.* 2022, 402, 117332.
25. Snider, D. An Incompressible Three-Dimensional Multiphase Particle-in-Cell Model for Dense Particle Flows. *J. Comput. Phys.* 2001, 170, 523–549.
26. Medina-Pedraza, C.; de Lasa, H. Hybrid Particle Cluster CPFD Simulation in the Acceleration and Stabilized Sections of a Downflow Circulating Fluidized Bed. *Ind. Eng. Chem. Res.* 2020, 59, 20325–20336.
27. Al-Sabawi, M.; Atias, J.A.; de Lasa, H. Kinetic Modeling of Catalytic Cracking of Gas Oil Feedstocks: Reaction and Diffusion Phenomena. *Ind. Eng. Chem. Res.* 2006, 45, 1583–1593.
28. Snider, D.M.; Clark, S.M.; O'Rourke, P.J. Eulerian–Lagrangian method for three-dimensional thermal reacting flow with application to coal gasifiers. *Chem. Eng. Sci.* 2011, 66, 1285–1295.
29. Oloruntoba, A.; Zhang, Y.; Xiao, H. Study on effect of gas distributor in fluidized bed reactors by hydrodynamics-reaction-coupled simulations. *Chem. Eng. Res. Des.* 2022, 177, 431–447.
30. Di Nardo, A.; Savuto, E.; Calchetti, G.; Stendardo, S. Computational particle fluid dynamics 3D simulation of the sorption-enhanced steam methane reforming process in a dual fluidized bed of bifunctional sorbent-catalyst particles. *Powder Technol.* 2023, 424, 118568.
31. Chang, S.-L.; Zhou, C.Q. Simulation of FCC riser flow with multiphase heat transfer and cracking reactions. *Comput. Mech.* 2003, 31, 519–532.
32. Arandes, J.M.; Azkoiti, M.J.; Bilbao, J.; de Lasa, H.I. Modelling FCC units under steady and unsteady state conditions. *Can. J. Chem. Eng.* 2000, 78, 111–123.
33. Behjat, Y.; Shahhosseini, S.; Marvast, M.A. CFD analysis of hydrodynamic, heat transfer and reaction of three phase riser reactor. *Chem. Eng. Res. Des.* 2011, 89, 978–989.
34. Du, Y.; Chen, X.; Li, S.; Berrouk, A.S.; Ren, W.; Yang, C. Revisiting a large-scale FCC riser reactor with a particle-scale model. *Chem. Eng. Sci.* 2022, 249, 117300.

35. Hajjar, Z.; Tayyebi, S.; Ahmadi, M.H.E. Application of AI in Chemical Engineering. In *Artificial Intelligence—Emerging Trends and Applications*; IntechOpen Ltd.: London, UK, 2018.
36. Venkatasubramanian, V. The promise of artificial intelligence in chemical engineering: Is it here, finally? *AIChE J.* 2019, 65, 466–478.
37. García, J.A.; Gómez, J.F.; Castellanos, N.T. Properties prediction of environmentally friendly ultra-high-performance concrete using artificial neural networks. *Eur. J. Environ. Civ. Eng.* 2022, 26, 2319–2343.
38. Du, C.; Han, C.; Yang, Z.; Wu, H.; Luo, H.; Niedzwiecki, L.; Lu, B.; Wang, W. Multiscale CFD Simulation of an Industrial Diameter-Transformed Fluidized Bed Reactor with Artificial Neural Network Analysis of EMMS Drag Markers. *Ind. Eng. Chem. Res.* 2022, 61, 8566–8580.
39. Lopez-Ramirez, E.; Lopez-Zamora, S.; Escobedo, S.; de Lasa, H. Artificial Neural Networks (ANNs) for Vapour-Liquid-Liquid Equilibrium (VLLE) Predictions in N-Octane/Water Blends. *Processes* 2023, 11, 2026.
40. Schubert, J.; Simutis, R.; Dors, M.; Havlik, I.; Lübbert, A. Bioprocess optimization and control: Application of hybrid modelling. *J. Biotechnol.* 1994, 35, 51–68.
41. Souza, P.V.d.C.; Lughofer, E.; Guimaraes, A.J. An interpretable evolving fuzzy neural network based on self-organized direction-aware data partitioning and fuzzy logic neurons. *Appl. Soft Comput.* 2021, 112, 107829.